Uncertainty of low-degree space gravimetry observations: surface processes versus internal signal

Hugo Lecomte[1], Séverine Rosat[1], Mioara Mandea[2], Jean-Paul Boy[1], Julia Pfeffer[3]

[1]Université de Strasbourg, CNRS, EOST, ITES UMR7063, F-67000 Strasbourg, France
[2]Centre National d'Etudes Spatiales, Paris, France
[3]Magellium, Ramonville Saint-Agne, France

Key Points:

- Deep Earth's processes occur at large spatial and inter-annual temporal scales
- Time-lapse gravity satellite data are compared with geophysical models at scales of interest
- Large uncertainties on satellite data and geophysical models conceal the gravity signals originated from the Earth's core

Corresponding author: Hugo Lecomte, `hlecomte@unistra.fr`

Abstract

Space gravity measurements have been mainly used to study the temporal mass variations at the Earth's surface and within the mantle. Nevertheless, mass variations due to the Earth's core might be observable in the variations of the gravity field as measured by GRACE and GRACE-FO satellites. Moreover, a possible correlation between the time-variable gravity and magnetic fields has been pointed out at inter-annual time scales. Earth's core dynamical processes inferred from geomagnetic field measurements are characterized by large-scale patterns associated with low spherical harmonic degrees of the potential fields. Studying Earth's core processes via gravity field observations involves the use of large spatial and inter-annual temporal filters. To access gravity variations related to the Earth's core, surface effects must be corrected, including hydrological, oceanic or atmospheric loading. This study estimates the uncertainty associated with gravity-field products and geophysical models used to minimise the surface process signatures in gravity field data. Here, we estimate the dispersion for GRACE solutions as about 0.34 cm of Equivalent Water Height (EWH) or 20% of the total signal. Uncertainty for hydrological models is as large as 0.89 to 2.10 cm of EWH. Loading products contain mostly different signals at inter-annuals time scales. We also show that a remaining hydrological signal in a very localized region can affect the low-degree components of the gravity field. The results presented here underline how challenging is to get new information about the dynamics of the Earth's core via high-accuracy gravity data.

Plain Language Summary

The motions of the Earth's fluid core are deduced from ground and satellite measurements of the geomagnetic field variations. Because the long-term variations of the Earth's gravity field might be correlated to the Earth's magnetic field, new information about the Earth's fluid core and its density changes could be accessed with gravimetry. The observation of the core processes must be done at very large spatial scales, in which case it is necessary to use gravity data from satellites. However, variations in the Earth's gravity field can also be created by heterogeneous superficial sources such as ocean and atmospheric currents, variations in water storage, etc. To recover a signature of the Earth's fluid core, we need first to remove all other known effects of larger amplitudes from satellite observations of the gravity field. Our study compares models of gravity variations for different sources in order to estimate their uncertainty.

1 Introduction

Gravity field variations measured by the Gravity Recovery and Climate Experiment (GRACE) and GRACE Follow-On (GRACE-FO) missions are sensitive to the redistribution of masses located above, at or below the Earth's surface (Chen et al., 2022). GRACE & GRACE-FO (referred to as GRACE) satellite data are used to estimate the Earth's mass variations from regional to global scales since 2002 (Tapley et al., 2004; Landerer et al., 2020). For example, GRACE satellite data became essential to monitor the evolution of terrestrial water storage, ice sheets, glaciers and sea level in a worldwide changing climate (Tapley et al., 2019). GRACE satellite data are, by nature, integrative, so that it may be difficult to separate the sources of change in the gravity field. Each process has a specific spatial and temporal signature that can go from global to local and from the secular to the sub-daily scales (Fig. 1). We refer to certain surface processes with the term "loading" defined here as the Newtonian attraction and mass redistribution associated with elastic deformation. By approximate order of magnitude, the processes include in GRACE records are tidal effects from extraterrestrial bodies, post-glacial rebound (Purcell et al., 2011), hydrological (Rodell et al., 2018), atmospheric (Kusche & Schrama, 2005) and oceanic (Dobslaw et al., 2017) loading, pre-seismic (Bouih et al., 2022), co-seismic and post seismic (Deggim et al., 2021) mass re-distributions, sea level changes (Adhikari et al., 2019; Horwath et al., 2022; Pfeffer et al., 2021) and finally core processes.

In addition to its primary purposes, some new applications of the GRACE measurements were proposed to study the deep Earth's interior. Panet et al. (2018) gave an example of possible seismic precursor in the mantle before Tohoku earthquake in 2011; this kind of signature was also observed before the Maule-Chile event (Bouih et al., 2022). Other authors have proposed to improve the knowledge of the dynamical processes of the Earth's core. Dumberry (2010a); Dumberry and Mandea (2021a) predicted a gravity perturbation generated by various core processes that might be observable on the low degrees of the gravity field. No signature of these perturbations has yet been observed in the gravity variations. However, Mandea et al. (2012) showed a correlation between the variations of the geomagnetic field and the gravity field. Processes of dissolution and crystallization at the core-mantle boundary (CMB) were advocated to explain this correlation (Mandea et al., 2015).

Established methods of seismic tomography, Earth's rotation, gravity and geomagnetic data analysis and geodynamic modelling constrain distributions of seismic velocity, density, electrical conductivity, and viscosity at depth, all depending on the internal structure of the Earth. Global Earth's interior models based on different observables often lead to rather different images. For example, the analysis of the time-variable magnetic field allows to focus on the dynamical features of the core field (Gillet et al., 2010). On the other hand, gaining information about the Earth's core from the analysis of the gravity field is difficult, because it requires to separate the different sources of signal with independent observations and/or models. In this context, gravimetry has the potential to bring new constraint about the density anomalies in the core and at its boundaries in a complimentary way to seismology (Koelemeijer, 2021).

Dynamical core processes disturb the gravity field through the direct Newtonian effect of mass anomalies in the liquid core, and through indirect effects, such as changes in the rotation vector of the solid Earth. Dumberry and Mandea (2021a) provided a review of the surface deformation and gravity variations induced by core dynamics, as well as a quantification of the expected amplitudes. Different mechanisms are covered including mass anomalies in the core, inner-core reorientation and pressure fluid acting at the CMB (Gillet et al., 2020). At spherical harmonic degree 2, the contribution of core processes to gravity variations and ground deformations is approximately 10 times smaller than the observed fluctuations caused by dynamical processes within the fluid layers at

the Earth's surface (Rosat et al., 2021). Consequently, extracting a signal of core origin remains challenging and requires an accurate removal of all surface effects.

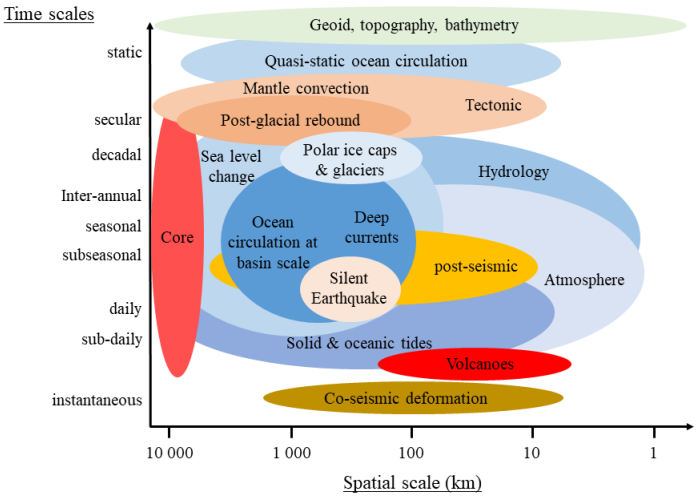

Figure 1: Spatial and temporal scales of the physical processes causing mass variations in the Earth system *adapted from Ilk et al. (2004)*

One way to extract the Earth's core signal from gravity observations is to use independent information from models of shallower sources (i.e. water mass redistribution in the hydrosphere, ocean, atmosphere, cryosphere and solid Earth's processes associated with earthquakes and glacial isostatic adjustment) to remove such larger amplitude contributions and to study the remaining signal. In this paper, we propose different models of post-glacial rebound, hydrological, atmospheric and oceanic mass redistribution for this purpose. The main objective of this work is to estimate the uncertainty associated with each category of models at large spatial scales over 1200 km and inter-annual time scales. This estimation can not be done for the earthquakes and for the cryosphere because the existing models are not independent from GRACE observations (Deggim et al., 2021; Adhikari et al., 2016).

To our knowledge, there was no published study evaluating gravity field products and models at these scales. A first paper in this direction has assessed the accuracy of satellite laser ranging (SLR) and hydrological loading products at inter-annual time-scales and for degree-2 as compared with surface deformation from GNSS (Rosat et al., 2021).

The objectives of this paper are first to present the satellite products and geophysical models used to estimate gravity variations (2). A minimum threshold of uncertainty is provided for each category of products and models (3). These uncertainties are finally discussed and compared with expected amplitudes of various core processes (4).

2 Data presentation

Solutions for the time-variable gravity field are obtained using GRACE measurements with SLR measurements for low degrees. Geophysical models representing hydrological, oceanic and glacial isostatic adjustment (GIA) processes are obtained from independent models and not from GRACE inputs.

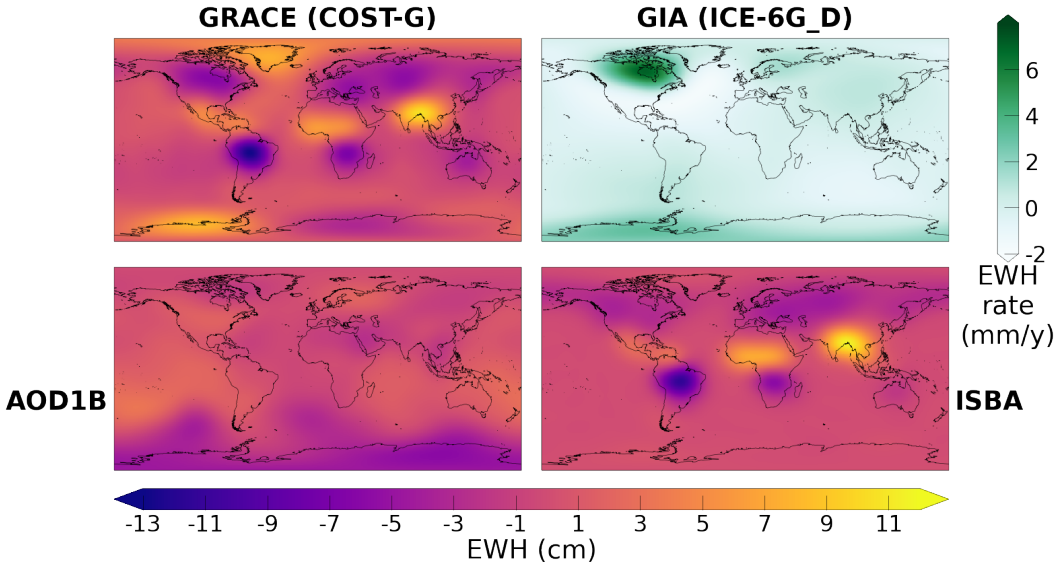

Figure 2: Surface mass in September 2008 estimated with the GRACE solution from the COST-G center (top left panel), the atmospheric and oceanic circulation model AOD1B (bottom left panel), the hydrological model Interaction Sol-Biosphère-Atmosphère (ISBA) (bottom right model) and GIA rate height change from ICE-6G_D model; a spatial filtering as detailed in 2.1.

2.1 Mathematical approach

Models and solutions are provided in either spherical harmonics (SH) or grid representation (Swenson & Wahr, 2002). Since we are interested in large spatial scales, we primarily use SH processing and representation. We only use the grid format to represent our results in a geographically interpretable way. Spatial representations are presented in Equivalent Water Height (EWH) (Fig. 2).

To study hypothetical gravity variations originating from the Earth's core, we filter the products and models considered in this study at specific spatial and temporal scales. The spatial filtering is done with a Gaussian filter (Jekeli, 1981) of radius 1200 km to access large spatial scales. We do not use the usual isotropic spatial filter (Kusche, 2007) that allows to recover high resolution signals. Post-filtered SH are increasingly reduced to degree 12 because of the Gaussian (Fig. 3). The temporal filtering is done with a Butterworth low-pass filter and a cutoff period at 2 years. This removes high-amplitude signals with annual and semi-annual periods in the products and models.

In the following, we note $C_{l,m}$ and $S_{l,m}$ the degree-l, order-m fully normalized Stokes coefficients of the SH representation of the Earth's gravitational potential. With $\hat{C}_{l,m}$ and $\hat{S}_{l,m}$ the unnormalized coefficients and $\delta_{m,0}$ the Kronecker delta, the normalization is given by:

$$\begin{bmatrix} C_{l,m} \\ S_{l,m} \end{bmatrix} = \sqrt{\frac{(n+m)!}{(2-\delta_{m,0})(2n+1)(n-m)!}} \begin{bmatrix} \hat{C}_{l,m} \\ \hat{S}_{l,m} \end{bmatrix} \quad (1)$$

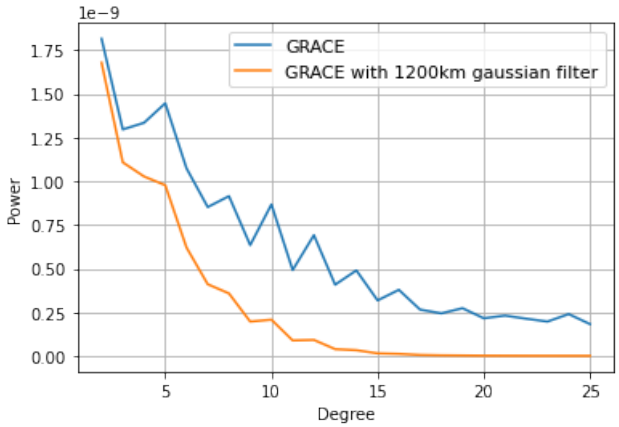

Figure 3: Power of SH degree for GRACE with and without spatial filtering up to degree 25

2.2 GRACE

GRACE gravity-field SH solutions are distributed by several analysis centers, providing GRACE Satellite-only Model (GSM) coefficients of the geopotential (Bettadpur, 2018). In this study, we considered 6 GSM solutions (see 1 for details) from the 3 Science Data System centers (Center for Space Research (CSR) (*CSR RL6.0*, 2018), German Research Centre for Geosciences (GFZ) (Dahle et al., 2019) and Jet Propulsion Laboratory (JPL) (*JPL RL6.0*, 2018)) and 3 non-official centers (International Combination Service for Time-variable Gravity Fields (COST-G) (Meyer et al., 2020), Institute of Geodesy at Graz University of Technology (IFG-TU GRAZ) (Mayer-Gürr et al., 2018) and Centre national d'études spatiales (CNES) (Lemoine et al., 2019)). GRAZ and CNES centers propose different approaches: sub-monthly hydrological de-aliasing for GRAZ, addition of SLR inputs for low degree determination for CNES. COST-G is a combination of the solutions from the other 5 centers used in this paper with the addition of Astronomical Institute University Bern (AIUB) solution. Detailed information about considered solutions are given in Table 1.

The 6 GRACE solutions considered in this study have a quasi-monthly time resolution. Time series span from the start of the GRACE mission, April 2002, to April 2021. There is a gap of one year between mid-2017 and mid-2018 between the GRACE and the GRACE-FO missions. As we are interested in the low degrees of the gravity field variations, we use only spherical harmonics (SH) models and not mascon products. SH solutions are global whereas mascon products are designed to access higher spatial resolution with pre-established grid that are an a priori of the mass distribution (Scanlon et al., 2016). Others institutes propose GRACE solutions, but they are not considered here.

The $C_{2,0}$ estimation with GRACE data is affected by a disturbing 161-day periodic signal (Chen et al., 2005; Cheng & Ries, 2017) without a consensual explanation for this issue. It has then become a standard to replace the GRACE determination of $C_{2,0}$ by the SLR one. We use the Technical notes TN14 solution based on SLR data and recommended in Loomis et al. (2019). The GRACE $C_{3,0}$ is also poorly observed when the satellites pair is operating without two fully functional accelerometers (Loomis et al., 2020). The TN14 solution also provides a $C_{3,0}$ estimation that we include after October 2016 (GRACE month $>$ 178). These two problematic estimations are suspected to also affect other coefficients such as $C_{4,0}$, $C_{5,0}$ and $C_{6,0}$ (Cheng & Ries, 2017; Sośnica

Table 1: Characteristics of the GRACE gravity-field models

Model	Mean Gravity Field Model	Ocean Tides	Atmospheric mass variations	Oceanic non-tidal mass variations	Data sources	Reference
CSR RL06	GGM05C	GOT4.8	AOD1B RL06 GAA	AOD1B RL06 GAB	`https://podaac-tools.jpl.nasa.gov/drive/`	(*CSR RL6.0*, 2018)
GFZ RL06	GGM05C	FES2014b	AOD1B RL06 GAA	AOD1B RL06 GAB	`https://podaac-tools.jpl.nasa.gov/drive/`	(Dahle et al., 2019)
JPL RL06	EIGEN-6C4	FES2014	AOD1B RL06 GAA	AOD1B RL06 GAB	`https://podaac-tools.jpl.nasa.gov/drive/`	(*JPL RL6.0*, 2018)
ITSG-Grace2018	ITSG-GraceGoce2017	FES2014b + GRACE estimates	AOD1B RL06 GAA and LSDM for sub-monthly hydrology de-aliasing	AOD1B RL06 GAB	`https://icgem.gfz-potsdam.de/`	(Mayer-Gürr et al., 2018)
CNES RL05	EIGEN-GRGS.RL04.MEAN-FIELD	FES2014b	3-D ECMWF ERA-Interim + AOD1B RL06 GAA	TUGO + AOD1B RL06 GAB	`https://grace.obs-mip.fr/`	(Lemoine et al., 2019)
COST-G RL01	X	X	X	X	`https://icgem.gfz-potsdam.de/`	(Meyer et al., 2020)

et al., 2015; Loomis et al., 2020). However, the quality of these GRACE coefficients is comparable with the quality of the SLR coefficient estimation (Cheng & Ries, 2017; Velicogna et al., 2020). It seems then not relevant to replace these coefficients. Dahle et al. (2019) suggested to have a special attention to $C_{2,1}$ and $S_{2,1}$ coefficients that contain an anomaly correlated with a failure of the accelerometers. We choose to replace these two coefficients with the SLR solution from Cheng et al. (2011) after October 2016. These replacements are not included in the CNES solution because it already includes SLR data at low degrees. Geocenter coefficients $C_{1,0}$, $C_{1,1}$ and $S_{1,1}$ are not included in our data and are set to 0 for the CNES solution where they come from SLR.

Few studies offer a comparison between solutions from different centers but not at our scales of interest. For example, Kvas et al. (2019) compared the GRAZ solution with those from CSR, GFZ and JPL in terms of temporal Root Mean Square (RMS) over a grid, quiet RMS time series and 161-day signal. Wang et al. (2021); Dobslaw et al. (2020) compared the estimations of global mean ocean mass and mean barystatic sea level with solutions from different centers. Blazquez et al. (2018) compared the trends of the global water budget components from 5 GRACE centers. It also estimated the uncertainties associated with the processing parameters, namely, the geocentre motions, $C_{2,0}$, filtering, leakage and GIA. In the following, we compare GIA, hydrology and non-tidal oceanic models.

2.3 Glacial Isostatic Adjustment (GIA)

The GIA signal induces linear trends in the gravity field variations. Effects of the post-glacial rebound are apparent in Antarctica, Northern America and Scandinavia. This signal rectification uses GIA models based on global ice-loading history and mantle viscosity. We do not consider regional GIA models since they would give spurious estimates of the GIA signal out of the specific regions for which they have been designed (Whitehouse et al., 2012). Present-day ice melting is not taken into account in the post-glacial rebound models, it hence constitutes another source of uncertainty.

We compare three different global GIA models, namely A13 (Geruo et al., 2013), ICE-6G_D (VM5a) (Peltier et al., 2018) and Caron18 (Caron et al., 2018).

A13 is based on the ICE5G ice-loading history model (Peltier, 2004) and on the multilayered viscosity profile VM2 (Peltier, 2004). A13 is computed via a 3-D finite-element method that creates a 3-D viscosity structure. ICE-6G_D uses an update of ICE5G ice-

load history with the addition of GNSS constraints. ICE-6G_D includes a more recent viscosity profile VM5a. Caron18 represents the mean of an ensemble of 128,000 forward models calculated in a Bayesian framework. For each run model, the viscosity structure and the scaling coefficients for the ice-load history of the Australian National University (ANU) model (Lambeck et al., 2010, 2014) vary. The final Caron18 GIA is a weighting of each model inferred by the probabilistic information and contains an estimate of the uncertainty from the dispersion between the models. A synthesis of these models is available in Table 2.

Table 2: Main characteristics of the GIA models

Model	Ice History	Viscosity Model (VM)	Lateral Heterogeneity	GNSS data
A13	ICE5G	VM2	Yes	No
ICE-6G_D	ICE6G	VM5a	No	Yes
Caron18	From ANU	Bayesian mean VM	No	Yes

Global GIA models are not associated with any uncertainty except for Caron18 and studies rarely discuss that point (Caron et al., 2018; Melini & Spada, 2019). A way of estimating the impact of the uncertainty of those models is by comparing some of them for a specific application. Śliwińska et al. (2021) used two different GIA models to estimate polar motion while Blazquez et al. (2018) compared three GIA models for the determination of global ocean mass change and sea level budget. In the case of regional applications, Kappelsberger et al. (2021) compared three global and two regional models with the uplift estimation from GNSS on the north-east of Greenland. However, to the best of our knowledge, there is no comparative study of GIA models based on the SH approach that was published, and more specifically, on low SH degrees.

2.4 Hydrology

We compare five global hydrological models, namely the Global Land Data Assimilation System Noah 2.1 (GLDAS) (Rodell et al., 2004), ERA5 (Hersbach et al., 2020), WaterGAP Global Hydrology Model version 2.2d (WGHM) (Döll et al., 2003), Interaction Sol-Biosphère-Atmosphère CNRM version of TRIP (ISBA-CTRIP, further referred to as ISBA) (Decharme et al., 2019) and Hydrological Land Surface Discharge Model (LSDM) (Dill, 2008). Hydrological models contain mainly annual and semi-annual signals. With the temporal and spatial filtering to access the core-like scales, the residuals studied are small compared to the original signals. For example, the RMS value of ISBA over continent is 3.64 cm in EWH and 1.47 cm EWH after temporal filtering. These residuals contain climatic modes like El Niño-Southern Oscillation.

The five hydrological models considered solve the vertical water mass balance but only three of them also solve the lateral fluxes. The water mass balance is expressed as the Terrestrial Water Storage (TWS) anomaly.

For GLDAS, the permanently ice-covered areas have been masked out. GLDAS has a spatial resolution of 0.25^o per 0.25^o and a temporal resolution of 3 hours. ERA5 has the same temporal and spatial resolutions. ERA5 is the new global model from Copernicus Climate Change Service that replaces the ERA-Interim reanalysis (Dee et al., 2011). GLDAS uses Global Precipitation Climatology Centre (GPCC) V1.3 Daily Analysis (Adler et al., 2003) has precipitation model. GPCC is a family of precipitation models based on in situ raingauge data to estimate monthly precipitation. For these two models, grav-

itational potential changes induced by hydrological mass redistribution and loading are computed as detailed in Petrov and Boy (2004) and Gégout et al. (2010).

WGHM, ISBA and LSDM are also supplemented with lateral fluxes solving. We use the variant IRR100 of WGHM forced with GPCC monthly V7.0 precipitation (Schneider et al., 2016). The output of the WGHM that we use in this study was already at a monthly-averaged temporal scale and the spatial resolution is 0.5^o. ISBA-CTRIP is the combination of a water balance model (ISBA) with a runoff model (CTRIP). ISBA has a temporal resolution of 3 hours and a spatial resolution of 1^o and it also uses GPCC V6 as a precipitation model. LSDM has a daily temporal frequency and a spatial resolution of 1^o. LSDM has been designed for large spatial scale geodetic applications such as the study of Earth's polar motion (Dill et al., 2010; Jin et al., 2012). Among the three models, only WGHM includes human-induced effects of freshwater resources. This contribution is extremely important when accounting for the contribution of freshwater fluxes to the global ocean (Schmied et al., 2020).

Table 3: Characteristics of the hydrological models

Acronym	Precipitation model	Sampling period	Space resolution
ERA5	Simultaneously generate	1 h	0.25^o
GLDAS	GPCP	3 h	0.25^o
ISBA	GPCC	3 h	1^o
WGHM	GPCC	monthly average	0.5^o
LSDM	ECMWF	daily	1^o

Each models have been resampled to a monthly time scale with an average over the month. The time coverage of comparison goes from 2002 to the end of 2016, this corresponds to the end of the WGHM model provided to us.

Previous studies compared hydrological models with GRACE gravity field variations but not with this diversity of models and at these inter-annual and large spatial scales (Lenczuk et al., 2020; Jin & Feng, 2013; Liu et al., 2019). At inter-annual and decadal scales, hydrological models compared with GRACE solution are underestimating the hydrological signal on river basins and regarding climate modes (Scanlon et al., 2018; Pfeffer et al., 2021).

2.5 Non-tidal oceanic loading

We compare three oceanic loading models, namely Ocean Model for Circulation and Tides (OMCT) (Dobslaw et al., 2013), Max-Planck-Institute for Meteorology Ocean Model (MPIOM) (Jungclaus et al., 2013) and Toulouse Unstructured Grid Ocean model (T-UGOm) (Carrere & Lyard, 2003). These models are used in GRACE solutions to correct for oceanic loading effects. For official centers, these models correspond to the GAB solution that contains the contribution of the dynamic ocean to ocean bottom pressure. OMCT has been used by official GRACE centers between Releases 1 and 5. MPIOM is used for the Release 6. T-UGOm is used by the CNES for the correction of the GRACE data (and not for GRACE-FO).

OMCT and MPIOM are baroclinic ocean models with a spatial resolution of 1^o. They are adjustments from another model, the climatological Hamburg Ocean Primitive Equation (HOPE) model. They are forced by external information from the operational analyses of the European Centre for Medium-Range Weather Forecast (ECMWF).

They compute water elevations, three-dimensional horizontal velocities, potential temperature and salinity. Both MPIOM and OMCT are forced by surface winds, pressure, atmospheric freshwater fluxes and surface temperature. MPIOM is using river runoff, sea-ice and corrects for the inverted barometer response of the oceans as opposed to OMCT. The T-UGOm barotropic ocean model is based on an unstructured grid with a higher resolution on coastal area. It does not represent variations of temperature and salinity but only displacement of the barotropic fluid. T-UGOm is using wind and atmospheric pressure forcing from ERA-interim and does not correct the inverted barometer response. Temporal and spatial resolutions of each model are detailed in Table 4.

Table 4: Characteristics of the ocean models

Acronym	Sampling period	Spatial resolution	Inverted barometer
OMCT	90 min	1^o	No
MPIOM	20 min	1^o	Yes
T-UGOm	3 hours	unstructured grid	No

To compare these three models we can not use the GAB solutions from GRACE releases because of the difference in the correction of the inverted barometer effect. The GAB solution for AOD1B RL06 with MPIOM uses the correction of the inverted barometer effect. It implies that the AOD1B RL06 GAA solution, which corresponds to the atmospheric loading effect, is equal to a constant value over oceanic area. For OMCT and T-UGOm, the GAB solution contains the inverted barometer effect and the GAA solution does not contain the inverted barometer effect. Regarding this, we compare the GAC solutions which are in fact the sum of the GAB (ocean loading) and the GAA (atmospheric loading) solutions over the ocean. This sum over oceanic areas corresponds to the oceanic bottom pressure and is given by the GAD solution in GRACE releases. To compare these oceanic loading models, the best way is to use the related GAD solutions.

Previous studies compared these models but at sub-monthly time scales (Bonin & Save, 2019; Dobslaw et al., 2015). Schindelegger et al. (2021) also compared some other oceanic models with MPIOM at sub-monthly time scales. We did not include these other models because some are in-house products and other are GRACE-dependent.

3 Comparison of gravity field solutions and models

In our approach, we cannot directly estimate the accuracy of solutions and models. We use an ensemble approach where the dispersion between solutions and models provides an estimate of the uncertainty. This estimate is a first lower bound that does not take into account any bias. This approach is similar to Blazquez et al. (2018) or Marti et al. (2022).

Comparisons between solutions and models are quantified as the Root Mean Square (RMS) difference between both objects weighted by latitude. In order to compute the weighted RMS, solutions and models are projected on a grid of $0.5^o \times 0.5^o$ degree and we compute the difference between the grids.

3.1 Differences between GRACE solutions

3.1.1 GRACE analysis centers

Comparison between GRACE solutions requires to minimize side effects due to the temporal filtering. We hence remove the first and last three months of the solutions.

	JPL	GFZ	GRAZ	CNES	COSTG	RMS
CSR	0.17	0.35	0.32	0.45	0.16	1.82
JPL		0.32	0.31	0.45	0.16	1.81
GFZ			0.45	0.53	0.30	1.82
GRAZ				0.45	0.27	1.87
CNES					0.42	1.86
COSTG						1.81

Table 5: RMS differences in cm EWH between different GRACE solutions and RMS value of each model after spatial and temporal filtering

Table 5 contains the RMS differences in cm EWH between the spatially and temporally filtered GRACE solutions from different analysis centers. For reference, the RMS value of the CSR solution is 1.82 cm EWH. The first group, CSR, JPL and COST-G solutions, is the most similar with an RMS difference of 0.16-0.17 cm EWH or 9% of the original RMS value for one solution. There is an increase of the difference to 0.22 cm EWH in 2016 at the end of GRACE lifespan corresponding to the accelerometer failure of one of the two satellites. Then comes a second group with GFZ and GRAZ which have an RMS difference of 0.3 cm EWH with the first group or 17% of the original RMS value for one solution. But the difference of these two solutions with the first group is different according to the considered epoch. GFZ has a peak going up to 0.7 cm EWH at the end of the GRACE lifespan. For GRAZ, in this temporal period, the difference goes up to 0.5 cm EWH but then it goes to 0.7 cm EWH at the end of the GRACE-FO time series. For the GFZ, the spatial distribution of differences corresponds to a global noise without any specific pattern. But for the GRAZ solutions, differences are located in areas of large signals, in the Amazon basin and Greenland. The CNES solution has a RMS difference of 0.45 cm EWH (25% of the original RMS value) with respect to other solutions with a temporal difference of 1 cm EWH at the beginning of the GRACE mission and at the end of the GRACE life span. The spatial localisation of these differences are located in areas of strong hydrological signal like the Amazon basin and India. Figures to illustrate these analyses are available in Appendix A.

3.1.2 GIA models

Figure 4 represents the difference in rate of EWH in mm per year between the models with a spatial resolution of 2400 km after a truncation at degree 60 and the application of a Gaussian filter. In Appendix B, the same figure without spatial filtering is available.

The models are similar in Scandinavia. The Caron18 model differs from the others in North America. The A13 model differs from the others in Antarctica and has small differences with the ICE-6G_D model in North America.

In North America, the disagreement between models goes up to 6 mm in EWH per year. In Antarctica, the differences between models are up to 10 mm in EWH per year.

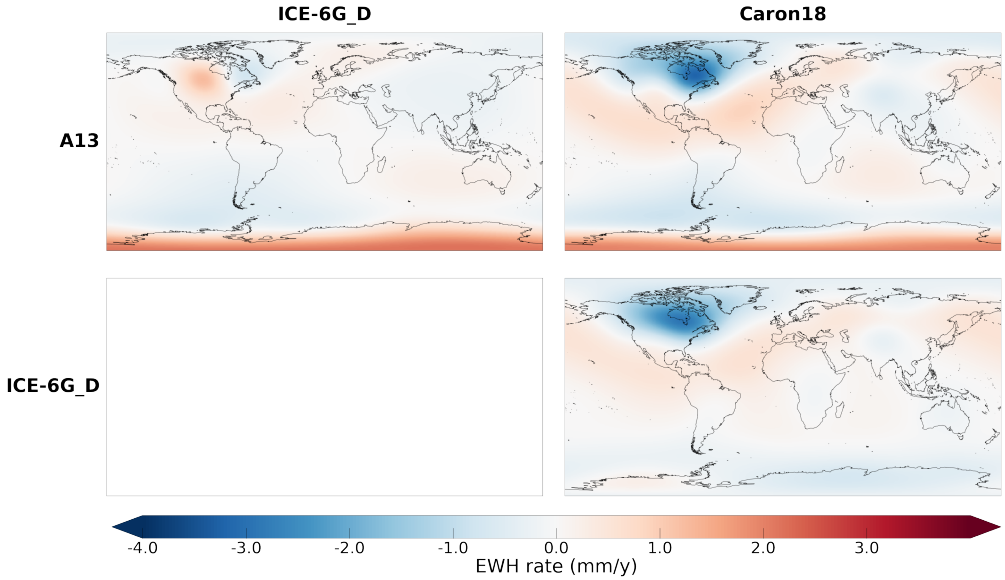

Figure 4: Difference between GIA models spatially filtered in EWH rate (mm/y)

These differences in velocity are currently accumulated over 20 years and at the time of publication of this article, they lead to a potential error of 12 cm in EWH per year over Antarctica and of 20 cm in EWH per year over North America.

3.1.3 Hydrological models

	GLDAS	ISBA	WGHM	LSDM	RMS
ERA5	0.89	0.89	1.36	1.50	0.91
GLDAS		0.89	1.20	1.74	1.26
ISBA			1.13	1.56	1.00
WGHM				2.10	1.36
LSDM					1.66

Table 6: RMS difference in cm EWH between hydrological models and RMS value of each model after spatial and temporal filtering over the continents

Table 6 contains the RMS differences in cm EWH between spatially and temporally filtered hydrological loading models (Newtonian attraction and mass redistribution associated with elastic deformation) over continents without Greenland and Antarctica. The RMS difference goes from 0.89 to 2.10 cm EWH or 100% to 155% of the original RMS value for one model. For example, the RMS values of ISBA and LSDM are respectively 1.00 and 1.66 cm EWH.

Because hydrological models take into account different processes, they yield very different TWS anomalies, leading to large differences in the predicted gravity variations at large spatial and temporal scales. At inter-annual and large spatial scales, ERA5, GLDAS and ISBA display relatively similar signals (Fig. 5a). Probably because it takes into ac-

count anthropogenic use of freshwater, WGHM exhibits larger differences, with larger TWS changes at inter-annual signals located in India and in the northern hemisphere than the other models (Fig. 5c).

LSDM shows the largest difference with other models. It has a very strong signal over the Nile area in North Africa (Fig. 5b). The difference between LSDM and other hydrological models like GLDAS has been documented and explained by the particular river channels redistribution of water (Dill & Dobslaw, 2013; Dill et al., 2018).

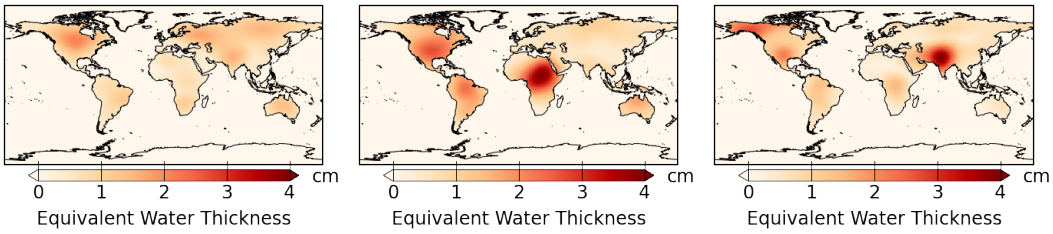

(a) ERA5 minus GLDAS

(b) ISBA minus LSDM

(c) ISBA minus WGHM

Figure 5: Maps of RMS difference between hydrological models over the continents after spatial and temporal filtering

The same analysis has been done on hydrological loading model without spatial filtering in Appendix C1.

The quality of hydrological loading models is in-equal. To evaluate this quality we look at the percentage of RMS explained by the models in the variation of the gravity field. We compare, over the continents, the RMS of the GRACE time series (COST-G) with the RMS of GRACE minus a hydrological model. The variation of the RMS value gives the percentage of RMS explain by the model in the GRACE time series (Table 7).

	ERA5	GLDAS	ISBA	WGHM	LSDM
Percentage (%)	7	0	24	21	-16

Table 7: Percentage of RMS explain by hydrological models in the GRACE time series at inter-annual scales with a spatial filtering

At inter-annual and large spatial scales, ISBA and WGHM reduce the variance of GRACE solutions by more than 20%. According to this criteria they have the best quality among the five models considered. ERA5 and WGHM are close to 0% and LSDM is negative with -16%. It does not modelize gravity field variations in GRACE time-series and contains other signals.

3.1.4 Non-tidal oceanic loading models

Table 8 contains the RMS differences in cm EWH between spatially and temporally filtered oceanic and atmospheric loading products over the oceans. The RMS difference goes from 0.33 to 0.45 cm EWH between models or 79% to 107% of the origi-

	MPIOM	T-UGOm	RMS
OMCT	0.33	0.45	0.42
MPIOM		0.42	0.39
T-UGOm			0.44

Table 8: RMS difference in cm EWH between oceanic loading products and RMS value of each model after spatial and temporal filtering over the oceans

nal RMS value for one model. For comparison, the RMS value for OMCT is 0.42 cm EWH. Because oceanic loading models come from different climate and fluid mechanics models, they have a very different spatial and temporal content, leading to large differences. Differences are mostly located in Arctic and Antarctic areas, coastal regions and in the Antarctic Circumpolar Current area (Fig. 6). OMCT has more signal in the Arctic while MPIOM and T-UGOm have more signal near Antarctica in the Ross Sea (Fig. 6).

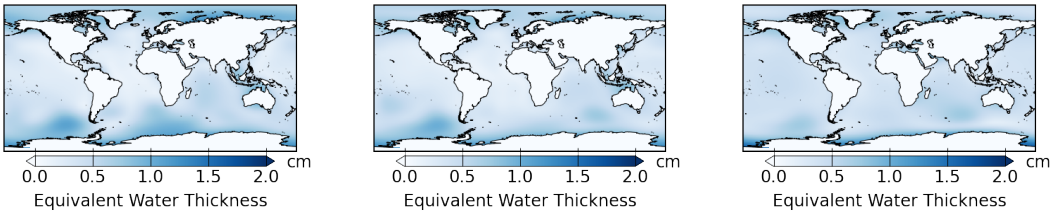

(a) OMCT (b) MPIOM (c) T-UGOm

Figure 6: Maps of RMS for oceanic loading products after spatial and temporal filtering over the oceans

There is another difference between these models: they are monthly products with potential missing days each month. These missing days correspond to low quality data but may vary between models and releases. This is the case for months at the beginning and at the end of the GRACE mission in 2002 and between 2012 and 2017. For example, for the month of August 2016, the MPIOM products from official centers contain measurements from days of year 221 to 247 while the T-UGOm products from the CNES contain measurements from days of year 214 to 244.

The same analysis has been done for oceanic loading models without spatial filtering (Appendix D1).

3.2 Impact of geophysical corrections on Stokes coefficients

We have quantified the uncertainties of GRACE solutions and correction models in terms of RMS of the differences over grids. Another interesting approach is to look at SH coefficients. Dumberry and Mandea (2021a) predicted that a potential core signal might be present from degree 2 onward to higher degrees with decreasing amplitudes.

To estimate the impact of an error in a model on specific SH coefficients, we have performed some synthetic test. An artificial synthetic signal is added to the GRACE gravity data on a bounded area. We study the effects of this synthetic signal on the retrieved

Stokes coefficients in terms of RMS value. To compare with the time-variable gravity measured by GRACE, we normalized each SH coefficients by the standard deviation $\sigma_{l,m}^{GRACE}$ of the degree-l, order-m Stokes coefficient from the COST-G solution. We note $I_{l,m}$ the normalized RMS value of the coefficient of degree l and order m given by:

$$I_{l,m} = \frac{\sqrt{\frac{1}{n}\sum_{t} \Delta C_{l,m}(t)^2}}{\sigma_{l,m}^{GRACE}} \tag{2}$$

With t the index of the time vector. This representation gives an estimate of the contamination by an error on the correction model with respect to the corrected GRACE signal.

3.2.1 Impact of an error in the GIA model

To study the effect of adding a fiducial GIA rectification, we create three synthetic signals corresponding to errors seen in 3.1.2.

- A linear signal of 10 mm/y in EWH located in North America with latitude between 50^o and 70^o and longitude between -95^o and -65^o.
- A linear signal of 6 mm/y in EWH located in Antarctica with latitude under -80^o.
- A linear signal of 3 mm/y in EWH located in Antarctica with latitude under -70^o and longitude between -160^o and -30^o.

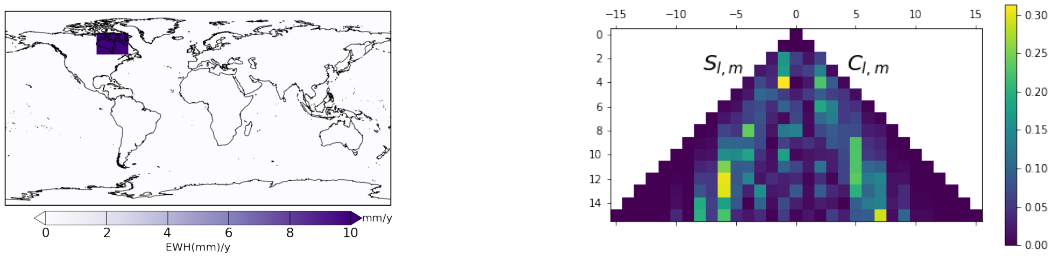

(a) Synthetic signal in North America in EWH

(b) SH power normalized by GRACE standard deviation up to degree 15

Figure 7: Effect of a 10 mm/yr trend in North America in the GIA model (a) on GRACE SH coefficients (b).

Introducing a 10 mm/y trend in North America alters the SH coefficients (Fig. 7). The error created on the GRACE $S_{4,1}$ coefficient by this fiducial reduction might be up to 30%. The other two synthetics experiments, with a trend at lower latitudes, affect the coefficients of orders 0 and 1 (Appendix E). The largest effect for a trend of 6 mm/y over Antarctica center is on $C_{8,0}$ with a trended bias of 50% of the GRACE RMS value. For a 3 mm/y trend in Antarctica between -160^o and -30^o in longitude, the effects are smaller with 15% of the GRACE RMS value on $S_{6,1}$ and $S_{8,1}$ (Appendix E).

3.2.2 Hydrology

Three cases have been simulated with a sinusoidal signal of period 3 years. They correspond to the difference between hydrological models established in Table 6 with the size of large hydrological basins:

- A sinusoidal signal of 4 cm in EWH over Africa (latitude between -10^o and 10^o, longitude between 10^o and 35^o).
- A sinusoidal signal of 3 cm in EWH over Amazonia (latitude between 0^o and 20^o, longitude between -70^o and -40^o).
- A sinusoidal signal of 4 cm in EWH over India (latitude between 20^o and 30^o, longitude between 70^o and 90^o).

The 3-year period was chosen arbitrarily and represents a residual hydrological signal.

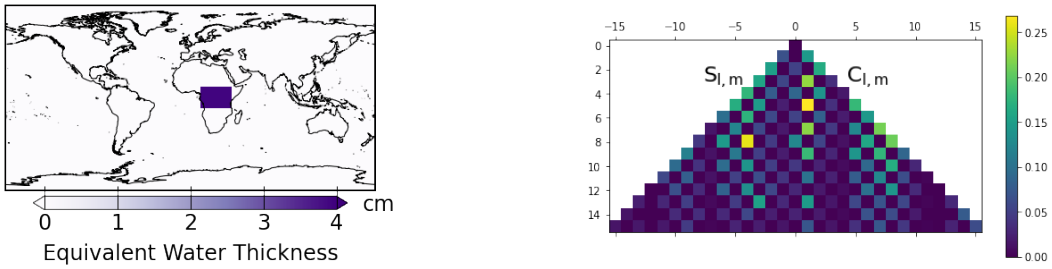

(a) Synthetic 3-yr signal over Africa with an amplitude of 4 cm EWH

(b) SH power normalized by GRACE standard deviation up to degree 15

Figure 8: Effect of a sinusoidal signal over Africa (a) on GRACE SH coefficients (b)

A 4-cm sinusoidal signal over Africa affects $C_{5,1}$ and $S_{8,4}$ by an amount of 25% of the GRACE RMS value (Fig. 8). A 3 cm sinusoidal signal over Amazonia affects $C_{4,3}$ and $S_{2,2}$ by an amount of 20%, while a 4 cm signal over India affects $C_{8,7}$ and $S_{8,6}$ by an amount of 10% (Appendix F).

4 Discussions & Conclusions

We presented different GRACE solutions, GIA and loading models. We compared each family of products with respect to the RMS difference. From this, we gave an estimate of their uncertainties and we characterized the possible effect on SH.

Type of data	Mean RMS difference (cm EWH)
GRACE solutions	0.34
Hydrological loading models	1.32
Oceanic loading models	0.40

Table 9: Summary of the RMS difference between data

A summary of the orders of magnitude of the dispersion between the different solutions and models obtained in this article is given in Table 9. To resume the information from this table:

- GRACE solutions are in good agreement with a dispersion that represents some 10 to 20% of the total signal, however, the agreement is not the same over the time

span covered by the two missions, with difference meanly at the beginning and end of each

- For hydrological loading models, the agreement is uneven (see also Fig. 5 & Table 6, 7). The dispersion between models is a large as the RMS value of models themselves. However, ISBA and WGHM are closer to GRACE solutions.
- For the oceanic loading models, the agreement is generally poor (see also Fig. 6). For each model, high-intensity signals are spatially located in different areas at inter-annual time scales. For example, T-UGOm is the only model to report large oceanic mass variations under the South of Africa.
- The GIA effects are not included in this recapitulating table as they are very localized in North America, Greenland and Antartica. To remind, GIA-mismodelled linear effects can go up to a 20 cm EWH after 20 years over North America. GIA errors will only impact the trend and not the inter-annual signals.

When models characterising surface processes are considered to minimise the signature of these processes in the gravity data, they might create some spurious signals on some areas. This would also create a spurious signal on specific SH (Fig. 7, Fig. 8) up to 50% of the total signal on inter-annual time scale.

Let us underline the importance of our results. Considering that the predicted core signals would have an amplitude of 10^{-11} for $C_{2,0}$ and 5×10^{-12} for other degree two coefficients (Dumberry, 2010b; Dumberry & Mandea, 2021b), they account respectively for 2 mm and 1 mm signals in EWH when projected onto the Earth's surface in a grid format. Dumberry and Mandea (2021b) also predicted a gravity signal in the $S_{2,2}$ coefficient with an amplitude below $2{\times}10^{-10}$ and at a time period around 10 to 30 years. The corresponding amplitude is below 2 cm in EWH at the Earth's surface. In this specific context, the RMS difference between GRACE solutions of 3.4 mm in EWH shows how difficult is to detect potential core signals. This difficulty is somehow reinforced when considering the use of loading models to minimize these components in the gravity signal, as the differences between loading products are large and these products are not completely adapted to our purposes.

A careful analysis of the time-variable gravity field data needs to be done for detecting signals from the core processes. Firstly, the data-gap between GRACE and GRACE-FO should be filled to ensure continuity and to improve the products quality (Richter et al., 2021). The largest signals in GRACE-kind solutions are due to the Earth's surface processes. The inter-annual variability analysis trough climate modes (Pfeffer et al., 2021) needs also to be considered. In order to detect tinny signals related to the core more sophisticated methods are needed such as empirical orthogonal function analysis (Schmeer et al., 2012) or independent component analysis (Frappart et al., 2011). Recently, (Saraswati et al., 2022) applied Singular Value Decomposition (SVD), Principal Component Analysis (PCA) and Multivariate Singular Spectrum Analysis (MSSA) to separate distinct spatio-temporal patterns in magnetic and gravity field. Moreover, synthetic tests have be performed to evaluate the sensitivity of these methods with respect of the Earth's core signals.

Both gravity and magnetic fields are complex, with a wide range of temporal and spatial variations and to describe them new models are needed. Only by modelling and interpreting multiple data sets a multifaceted image of the true structure of the Earth can be obtained.

5 Supplementary materials

Appendix A Temporal variation of the RMS difference between various GRACE solutions

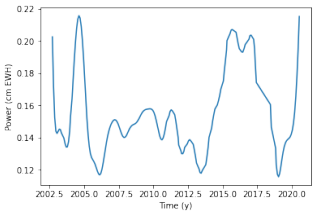

(a) Temporal RMS difference between CSR and COST-G solutions

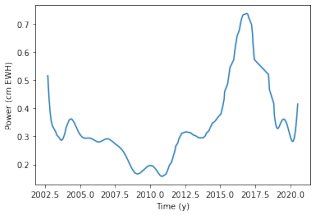

(b) Temporal RMS difference between CSR and GFZ solutions

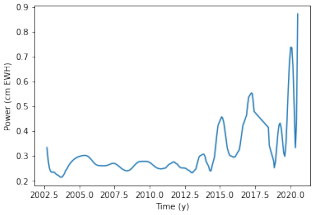

(c) Temporal RMS difference between CSR and GRAZ solutions

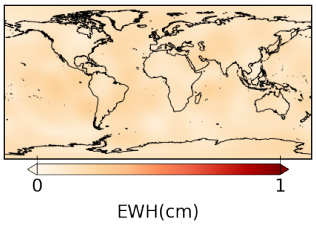

(d) Spatial RMS difference between CSR and JPL solutions

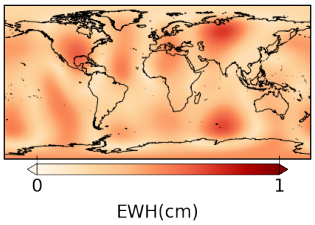

(e) Spatial RMS difference between CSR and GFZ solutions

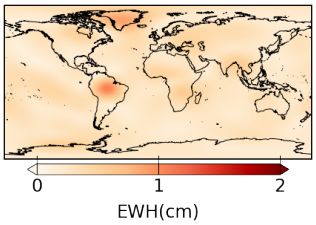

(f) Spatial RMS difference between CSR and GRAZ solutions

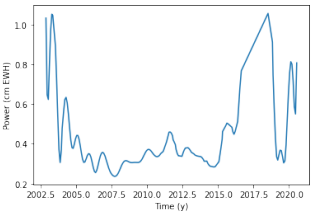

(g) Temporal RMS difference between CSR and CNES solutions

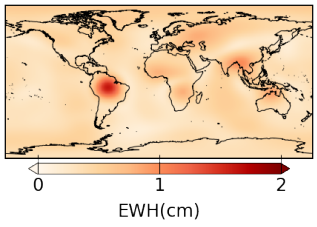

(h) Spatial RMS difference between CSR and CNES solutions

Figure A1: RMS difference between GRACE center solutions on temporal and spatial representation

Appendix B Difference between GIA models without spatial filtering

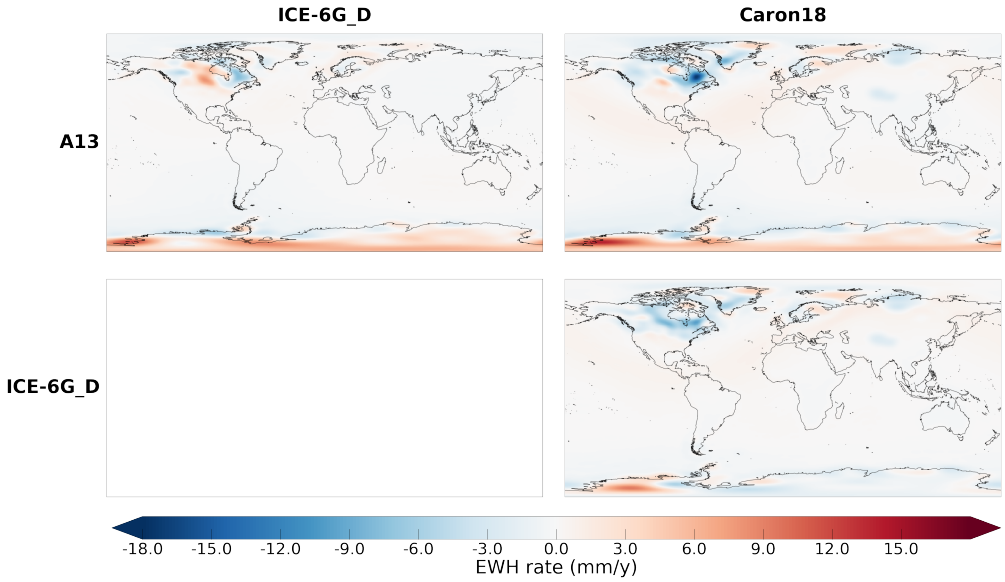

Figure B1: Difference of between GIA models in EWH rate (mm/y)

The amplitude of the GIA signal is five times larger without spatial filtering and the signal is more localize.

Appendix C Difference between hydrological loading with temporal filtering and without spatial filtering

	GLDAS	ISBA	WGHM	LSDM	RMS
ERA5	2.06	2.11	2.92	2.69	2.35
GLDAS		2.04	2.74	2.99	2.67
ISBA			2.55	2.66	2.43
WGHM				3.67	3.05
LSDM					2.47

Table C1: RMS difference in cm EWH between hydrological models and RMS value of each model after a temporal filtering

Table C1 contains the RMS difference in cm EWH between temporally filtered hydrological products over continents without Greenland and Antarctica. The RMS difference goes from 2.04 to 3.67 cm EWH between models. For example of comparison, the RMS value of ISBA and WGHM are respectively 2.43 and 3.05 cm EWH.

At inter-annual time scales, the models show different signals. For example, WGHM is the only one to contain a strong signal over India and North America, while LSDM is the only one to contain a signal over the Nile region in Africa. They do not correspond at all.

We can also note that the spatial filtering smooths the signal amplitude.

Appendix D Difference between oceanic loading with temporal filtering and without spatial filtering

	MPIOM	T-UGOm	RMS
OMCT	0.72	0.79	0.84
MPIOM		0.74	0.77
T-UGOm			0.52

Table D1: RMS difference in cm EWH between oceanic loading solutions and RMS value of each model after temporal filtering

Table D1 contains the RMS difference in cm EWH between temporally filtered oceanic and atmospheric loading products over the oceans. The RMS difference goes from 0.72 to 0.79 cm EWH between models. For comparison, the RMS value for OMCT is 0.84 cm EWH. This means that models are not in agreement at inter-annual scales and they represent very different signals.

Appendix E Cases n^o2 and n^o3 for GIA synthetic error effects

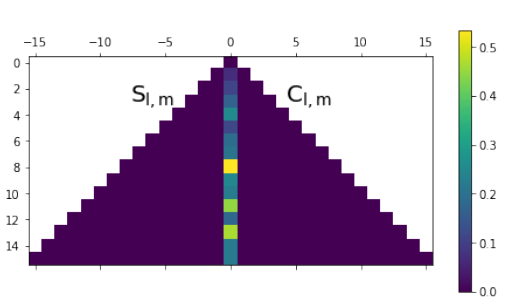

(a) Case n^o2 with synthetic signal under -80^o of latitude

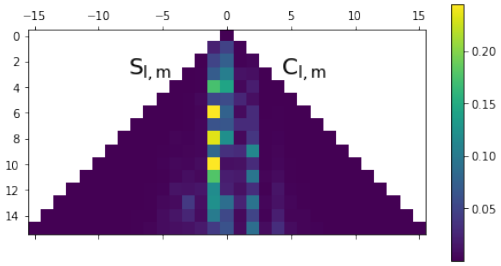

(b) Case n^o3 with synthetic signal under -70^o of latitude and between -160^o and -30^o of longitude

Figure E1: SH power normalized by GRACE standard deviation up to degree 15

Appendix F Cases n^o2 and n^o3 for synthetic error effects corresponding to hydrological loading

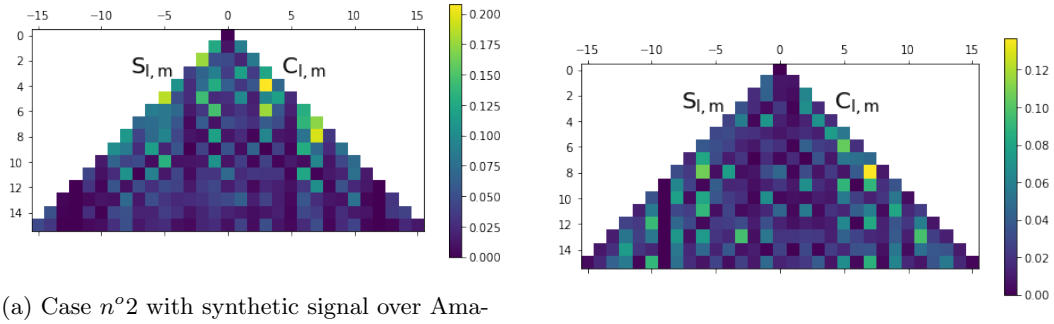

(a) Case n^o2 with synthetic signal over Amazon forest

(b) Case n^o3 with synthetic signal over India

Figure F1: SH power normalized by GRACE standard deviation up to degree 15

Acronyms

AIUB Astronomical Institute University Bern
CMB Core-Mantle Boundary
CNES Centre national d'études spatiales
CSR Center for Space Research
EWH Equivalent Water Height
GFZ German Research Centre for Geosciences
GIA Glacial Isostatic Adjustment
GLDAS Global Land Data Assimilation System
GRACE Gravity Recovery And Climate Experiment
GRACE-FO Gravity Recovery And Climate Experiment Follow-On
GSM GRACE Satellite-only Model
IFG TU Graz Institute of Geodesy at Graz University of Technology
ISBA Interaction Sol-Biosphère-Atmosphère
ISBA-CTRIP Interaction Sol-Biosphère-Atmosphère CNRM version of TRIP
JPL Jet Propulsion Laboratory
MPIOM Max-Planck-Institute for Meteorology Ocean Model
OMCT Ocean Model for Circulation and Tides
RMS Root Mean Square
SH Spherical Harmonics
SLR Satellite Laser Ranging
T-UGOm Toulouse Unstructured Grid Ocean model
TWS Total Water Storage
WGHM WaterGAP Global Hydrology Model

Acknowledgments

This work is supported by the Centre national d'études spatiales (CNES) and by the Doctoral School Earth and Environmental Sciences (ED 413) of the University of Strasbourg in the Institut Terre et Environnement de Strasbourg (ITES, UMR7063). This project

has received funding from the European Research Council (ERC) under the European Union's Horizon 2020 research and innovation program (GRACEFUL Synergy Grant agreement No 855677).

GRACE and GRACE-FO missions are sponsored by the National Aeronautics and Space Administration and the Deutsches Zentrum für Luft-und Raumfahrt. GRACE and GRACE-FO Level-2 temporal solutions were obtained from the PO.DAAC Drive for CSR, GFZ and JPL centers, from `https://icgem.gfz-potsdam.de/` for ITSG center, from `https://grace.obs-mip.fr/` for CNES center and from `https://icgem.gfz-potsdam.de/` for the COST-G combination. The GIA models were obtained from the PO.DAAC Drive (`http://grace.jpl.nasa.gov`). Time-variable gravity field coefficients due to hydrological loading can be downloaded from EOST loading service (`http://loading.u-strasbg.fr/`) for ERA5 and GLDAS models. LSDM model is available on the ESMGFZ Product repository (`http://rz-vm115.gfz-potsdam.de:8080`) and is produced by IERS Associated Product Centre Deutsches GeoForschungsZentrum GFZ Potsdam. The ISBA-CTRIP model made by the "Centre National de Recherches Météorologiques" (CNRM) of Météo-France has been provided by Bertrand Decharmes. The WGHM model (`http://www.watergap.de/`) has been provided by Denise Caceres from Frankfurt University. MPIOM and OMCT are available on the PO.DAAC Drive and T-UGOm model has been provided by the CNES.

Finally, the Python 3.8 code used for this publication is based on a Github project by Tyler Tsutterley (`https://github.com/tsutterley/read-GRACE-harmonics`). The adapted version can be found on `https://github.com/hulecom/read-GRACE-harmonics` repository.

References

Adhikari, S., Ivins, E. R., Frederikse, T., Landerer, F. W., & Caron, L. (2019, May). Sea-level fingerprints emergent from GRACE mission data. *Earth System Science Data*, *11*(2), 629–646. Retrieved 2022-07-21, from `https://essd.copernicus.org/articles/11/629/2019/` (Publisher: Copernicus GmbH) doi: 10.5194/essd-11-629-2019

Adhikari, S., Ivins, E. R., & Larour, E. (2016, March). ISSM-SESAW v1.0: mesh-based computation of gravitationally consistent sea-level and geodetic signatures caused by cryosphere and climate driven mass change. *Geoscientific Model Development*, *9*(3), 1087–1109. Retrieved 2022-07-21, from `https://gmd.copernicus.org/articles/9/1087/2016/` doi: 10.5194/gmd-9-1087-2016

Adler, R. F., Huffman, G. J., Chang, A. T. C., Ferraro, R., Xie, P., Janowiak, J. E., ... Nelkin, E. (2003). The version 2 global precipitation climatology project (gpcp) monthly precipitation analysis (1979-present). *Journal of Hydrometeorology*. doi: 10.1175/1525-7541(2003)004⟨1147:tvgpcp⟩2.0.co;2

Bettadpur, S. (2018). *Level-2 Gravity Field Product User Handbook* (User Handbook). Center for Space Research. Retrieved from `https://podaac-tools.jpl.nasa.gov/drive/files/allData/grace/docs/L2-UserHandbook_v4.0.pdf`

Blazquez, A., Meyssignac, B., Lemoine, J.-M., Berthier, E., Ribes, A., & Cazenave, A. (2018). Exploring the uncertainty in GRACE estimates of the mass redistributions at the Earth surface: implications for the global water and sea level budgets. *Geophysical Journal International*. doi: 10.1093/gji/ggy293

Bonin, J. A., & Save, H. (2019). Evaluation of sub-monthly oceanographic signal in grace "daily" swath series using altimetry. *Ocean Science Discussions*. doi: 10.5194/os-16-423-2020

Bouih, M., Panet, I., Remy, D., Longuevergne, L., & Bonvalot, S. (2022). Deep mass redistribution prior to the 2010 mw 8.8 maule (chile) earthquake revealed by grace satellite gravity. *Earth and Planetary Science Letters*, *584*, 117465.

Retrieved from https://www.sciencedirect.com/science/article/pii/S0012821X22001017 doi: https://doi.org/10.1016/j.epsl.2022.117465

Caron, L., Ivins, E. R., Larour, E., Larour, E., Adhikari, S., Nilsson, J., ... Blewitt, G. (2018). Gia model statistics for grace hydrology, cryosphere, and ocean science. *Geophysical Research Letters*. doi: 10.1002/2017gl076644

Carrere, L., & Lyard, F. (2003). Modeling the barotropic response of the global ocean to atmospheric wind and pressure forcing - comparisons with observations. *Geophysical Research Letters*. doi: 10.1029/2002gl016473

Chen, J., Cazenave, A., Dahle, C., Llovel, W., Panet, I., Pfeffer, J., & Moreira, L. (2022, February). Applications and Challenges of GRACE and GRACE Follow-On Satellite Gravimetry. *Surveys in Geophysics*, *43*(1), 305–345. Retrieved 2022-07-21, from https://doi.org/10.1007/s10712-021-09685-x doi: 10.1007/s10712-021-09685-x

Chen, J., Rodell, M., Wilson, C. R., & Famiglietti, J. S. (2005). Low degree spherical harmonic influences on gravity recovery and climate experiment (grace) water storage estimates. *Geophysical Research Letters*. doi: 10.1029/2005gl022964

Cheng, M., & Ries, J. C. (2017). The unexpected signal in grace estimates of c_{20}. *Journal of Geodesy*. doi: 10.1007/s00190-016-0995-5

Cheng, M., Ries, J. C., & Tapley, B. D. (2011). Variations of the earth's figure axis from satellite laser ranging and grace. *Journal of Geophysical Research*. doi: 10.1029/2010jb000850

CSR RL6.0. (2018). Retrieved from https://podaac.jpl.nasa.gov/dataset/GRACE_GSM_L2_GRAV_CSR_RL06

Dahle, C., Flechtner, F., Dobslaw, H., Michalak, G., Neumayer, K.-H., Reinhold, A., ... Sulzbach, R. (2019). The GFZ GRACE RL06 Monthly Gravity Field Time Series: Processing Details and Quality Assessment. *Remote Sensing*. doi: 10.3390/rs11182116

Decharme, B., Delire, C., Minvielle, M., Colin, J., Vergnes, J., Alias, A., ... Voldoire, A. (2019). Recent changes in the isba-ctrip land surface system for use in the cnrm-cm6 climate model and in global off-line hydrological applications. *Journal of Advances in Modeling Earth Systems*. doi: 10.1029/2018ms001545

Dee, D., Uppala, S., Simmons, A., Berrisford, P., Kobayashi, S., Andrae, U., ... Thépaut, J.-N. (2011). The era-interim reanalysis: configuration and performance of the data assimilation system. *Quarterly Journal of the Royal Meteorological Society*. doi: 10.1002/qj.828

Deggim, S., Eicker, A., Schawohl, L., Gerdener, H., Schulze, K., Engels, O., ... Longuevergne, L. (2021, May). RECOG RL01: correcting GRACE total water storage estimates for global lakes/reservoirs and earthquakes. *Earth System Science Data*, *13*(5), 2227–2244. Retrieved 2022-03-11, from https://essd.copernicus.org/articles/13/2227/2021/ (Publisher: Copernicus GmbH) doi: 10.5194/essd-13-2227-2021

Dill, R. (2008). Hydrological model lsdm for operational earth rotation and gravity field variations. *null*. doi: 10.2312/gfz.b103-08095

Dill, R., Dill, R., Dobslaw, H., & Dobslaw, H. (2010). Short-term polar motion forecasts from earth system modeling data. *Journal of Geodesy*. doi: 10.1007/s00190-010-0391-5

Dill, R., & Dobslaw, H. (2013). Numerical simulations of global-scale high-resolution hydrological crustal deformations. *Journal of Geophysical Research: Solid Earth*, *118*(9), 5008–5017. Retrieved 2022-06-23, from https://onlinelibrary.wiley.com/doi/abs/10.1002/jgrb.50353 (_eprint: https://onlinelibrary.wiley.com/doi/pdf/10.1002/jgrb.50353) doi: 10.1002/jgrb.50353

Dill, R., Klemann, V., & Dobslaw, H. (2018). Relocation of River Storage From Global Hydrological Models to Georeferenced River Channels for Improved Load-Induced Surface Displacements. *Journal of Geophysical Research: Solid Earth*, *123*(8), 7151–7164. Retrieved 2022-06-23, from https://onlinelibrary.wiley.com/doi/abs/10.1029/2018JB016141 (_eprint: https://onlinelibrary.wiley.com/doi/pdf/10.1029/2018JB016141) doi: 10.1029/2018JB016141

Dobslaw, H., Bergmann-Wolf, I., Dill, R., Poropat, L., Thomas, M., Dahle, C., ... Flechtner, F. (2017, October). A new high-resolution model of non-tidal atmosphere and ocean mass variability for de-aliasing of satellite gravity observations: AOD1B RL06. *Geophysical Journal International*, *211*(1), 263–269. Retrieved 2022-07-21, from https://doi.org/10.1093/gji/ggx302 doi: 10.1093/gji/ggx302

Dobslaw, H., Bergmann-Wolf, I., Forootan, E., Dahle, C., Mayer-Gürr, T., Kusche, J., & Flechtner, F. (2015). Modeling of present-day atmosphere and ocean non-tidal de-aliasing errors for future gravity mission simulations. *Journal of Geodesy*. doi: 10.1007/s00190-015-0884-3

Dobslaw, H., Dill, R., Dill, R., Bagge, M., Klemann, V., Boergens, E., ... Flechtner, F. (2020). Gravitationally consistent mean barystatic sea level rise from leakage-corrected monthly grace data. *Journal of Geophysical Research*. doi: 10.1029/2020jb020923

Dobslaw, H., Dobslaw, H., Flechtner, F., Bergmann-Wolf, I., Dahle, C., Dahle, C., ... Thomas, M. (2013). Simulating high-frequency atmosphere-ocean mass variability for dealiasing of satellite gravity observations: Aod1b rl05. *Journal of Geophysical Research*. doi: 10.1002/jgrc.20271

Dumberry, M. (2010a). Gravity variations induced by core flows. *Geophysical Journal International*, *180*(2), 635–650. Retrieved 2022-03-11, from https://doi.org/10.1111/j.1365-246X.2009.04437.x doi: 10.1111/j.1365-246X.2009.04437.x

Dumberry, M. (2010b). Gravity variations induced by core flows. *Geophysical Journal International*, *180*(2), 635–650.

Dumberry, M., & Mandea, M. (2021a). Gravity Variations and Ground Deformations Resulting from Core Dynamics. *Surveys in Geophysics*. Retrieved 2022-03-11, from https://doi.org/10.1007/s10712-021-09656-2 doi: 10.1007/s10712-021-09656-2

Dumberry, M., & Mandea, M. (2021b). Gravity variations and ground deformations resulting from core dynamics. *Surveys in Geophysics*, *accepted*.

Döll, P., Kaspar, F., & Lehner, B. (2003). A global hydrological model for deriving water availability indicators: model tuning and validation. *Journal of Hydrology*. doi: 10.1016/s0022-1694(02)00283-4

Frappart, F., Ramillien, G., Leblanc, M., Leblanc, M., Tweed, S., Bonnet, M.-P., & Maisongrande, P. (2011). An independent component analysis filtering approach for estimating continental hydrology in the grace gravity data. *Remote Sensing of Environment*. doi: 10.1016/j.rse.2010.08.017

Gégout, P., Boy, J.-P., Hinderer, J., & Ferhat, G. (2010). Modeling and observation of loading contribution to time-variable GPS sites positions. In *Gravity, geoid and earth observation* (pp. 651–659). Springer.

Geruo, A., Wahr, J., & Zhong, S. (2013). Computations of the viscoelastic response of a 3-D compressible Earth to surface loading: an application to Glacial Isostatic Adjustment in Antarctica and Canada. *Geophysical Journal International*. doi: 10.1093/gji/ggs030

Gillet, N., Dumberry, M., & Rosat, S. (2020). The limited contribution from outer core dynamics to global deformations at the Earth's surface. *Geophysical Journal International*, *224*, 216–229. doi: 10.1093/gji/ggaa448

Gillet, N., Lesur, V., & Olsen, N. (2010, August). Geomagnetic Core Field Secular Variation Models. *Space Science Reviews*, *155*(1), 129–145. Retrieved 2022-05-06, from https://doi.org/10.1007/s11214-009-9586-6 doi: 10.1007/s11214-009-9586-6

Hersbach, H., Bell, B., Berrisford, P., Hirahara, S., Horanyi, A., Munoz-Sabater, J., ... Thépaut, J.-N. (2020). The era5 global reanalysis. *Quarterly Journal of the Royal Meteorological Society*. doi: 10.1002/qj.3803

Horwath, M., Gutknecht, B. D., Cazenave, A., Palanisamy, H. K., Marti, F., Marzeion, B., ... Benveniste, J. (2022, February). Global sea-level budget and ocean-mass budget, with a focus on advanced data products and uncertainty characterisation. *Earth System Science Data*, *14*(2), 411–447. Retrieved 2022-07-21, from https://essd.copernicus.org/articles/14/411/2022/ (Publisher: Copernicus GmbH) doi: 10.5194/essd-14-411-2022

Ilk, K.-H., Flury, J., Rummel, R., Schwintzer, P., Bosch, W., Haas, C., ... Gravity Field and Gravimetry 2009, G. C. (2004). *Mass Transport and Mass Distribution in the Earth System : Contribution of the New Generation of Satellite Gravity and Altimetry Missions to Geosciences; Proposal for a German Priority Research Program* (Tech. Rep.). Retrieved 2022-06-22, from https://gfzpublic.gfz-potsdam.de/pubman/faces/ViewItemFullPage.jsp?itemId=item_231104_1 (Publisher: GOCE-Projektbüro Deutschland, Techn. Univ. München, GeoForschungsZentrum Potsdam)

Jekeli, C. (1981). Alternative methods to smooth the earth's gravity field. *null*. doi: null

Jin, S., & Feng, G. (2013, July). Large-scale variations of global groundwater from satellite gravimetry and hydrological models, 2002–2012. *Global and Planetary Change*, *106*, 20–30. Retrieved 2022-06-23, from https://linkinghub.elsevier.com/retrieve/pii/S0921818113000416 doi: 10.1016/j.gloplacha.2013.02.008

Jin, S., Hassan, A. A., & Feng, G. (2012). Assessment of terrestrial water contributions to polar motion from grace and hydrological models. *Journal of Geodynamics*. doi: 10.1016/j.jog.2012.01.009

JPL RL6.0. (2018). Retrieved from https://podaac.jpl.nasa.gov/dataset/GRACE_GSM_L2_GRAV_JPL_RL06

Jungclaus, J. H., Fischer, N., Haak, H., Lohmann, K., Marotzke, J., Matei, D., ... von Storch, J.-S. (2013). Characteristics of the ocean simulations in mpiom the ocean component of the mpi earth system model. *Journal of Advances in Modeling Earth Systems*. doi: 10.1002/jame.20023

Kappelsberger, M. T., Strößenreuther, U., Scheinert, M., Horwath, M., Groh, A., Knöfel, C., ... Khan, S. A. (2021). Modeled and observed bedrock displacements in north-east Greenland using refined estimates of present-day ice-mass changes and densified GNSS measurements. *Journal of Geophysical Research*. doi: 10.1029/2020jf005860

Koelemeijer, P. (2021). Toward consistent seismological models of the core–mantle boundary landscape. In *Mantle convection and surface expressions* (p. 229-255). American Geophysical Union (AGU). Retrieved from https://agupubs.onlinelibrary.wiley.com/doi/abs/10.1002/9781119528609.ch9 doi: https://doi.org/10.1002/9781119528609.ch9

Kusche, J. (2007). Approximate decorrelation and non-isotropic smoothing of time-variable grace-type gravity field models. *Journal of Geodesy*. doi: 10.1007/s00190-007-0143-3

Kusche, J., & Schrama, E. J. O. (2005). Surface mass redistribution inversion from global GPS deformation and Gravity Recovery and Climate Experiment (GRACE) gravity data. *Journal of Geophysical Research: Solid Earth*, *110*(B9). Retrieved 2022-07-21, from https://onlinelibrary.wiley.com/doi/abs/10.1029/2004JB003556 (_eprint:

https://onlinelibrary.wiley.com/doi/pdf/10.1029/2004JB003556) doi: 10.1029/2004JB003556

Kvas, A., Behzadpour, S., Ellmer, M., Klinger, B., Strasser, S., Zehentner, N., & Mayer-Gürr, T. (2019). Itsg-grace2018: Overview and evaluation of a new grace-only gravity field time series. *Journal of Geophysical Research: Solid Earth*, *124*(8), 9332-9344. Retrieved from https://agupubs.onlinelibrary.wiley.com/doi/abs/10.1029/2019JB017415 doi: https://doi.org/10.1029/2019JB017415

Lambeck, K., Purcell, A. W., Zhao, J., Zhao, J., & Svensson, N.-O. (2010). The scandinavian ice sheet: from mis 4 to the end of the last glacial maximum. *Boreas*. doi: 10.1111/j.1502-3885.2010.00140.x

Lambeck, K., Rouby, H., Purcell, A. W., Sun, Y., & Sambridge, M. (2014). Sea level and global ice volumes from the last glacial maximum to the holocene. *Proceedings of the National Academy of Sciences of the United States of America*. doi: 10.1073/pnas.1411762111

Landerer, F. W., Flechtner, F. M., Save, H., Webb, F. H., Bandikova, T., Bertiger, W. I., ... Yuan, D.-N. (2020). Extending the Global Mass Change Data Record: GRACE Follow-On Instrument and Science Data Performance. *Geophysical Research Letters*, *47*(12), e2020GL088306. Retrieved 2022-07-21, from https://onlinelibrary.wiley.com/doi/abs/10.1029/2020GL088306 (_eprint: https://onlinelibrary.wiley.com/doi/pdf/10.1029/2020GL088306) doi: 10.1029/2020GL088306

Lemoine, J.-M., Biancale, R., Reinquin, F., Bourgogne, S., & Gégout, P. (2019). *CNES/GRGS RL04 Earth gravity field models, from GRACE and SLR data.* GFZ Data Services. Retrieved from https://dataservices.gfz-potsdam.de/icgem/showshort.php?id=escidoc:4656890 (Type: dataset) doi: 10.5880/ICGEM.2019.010

Lenczuk, A., Leszczuk, G., Klos, A., Kosek, W., & Bogusz, J. (2020, October). Study on the inter-annual hydrology-induced deformations in Europe using GRACE and hydrological models. *Journal of Applied Geodesy*, *14*(4), 393–403. Retrieved 2022-06-23, from https://www.degruyter.com/document/doi/10.1515/jag-2020-0017/html (Publisher: De Gruyter) doi: 10.1515/jag-2020-0017

Liu, R., She, D., Li, M., & Wang, T. (2019). Using satellite observations to assess applicability of gldas and wghm hydrological model. *Geomatics and Information Science of Wuhan University*, *44*(1671?8860(2019)11?1596?09), 1596. Retrieved from http://ch.whu.edu.cn/en/article/doi/10.13203/j.whugis20190108 doi: 10.13203/j.whugis20190108

Loomis, B. D., Rachlin, K. E., & Luthcke, S. B. (2019). Improved earth oblateness rate reveals increased ice sheet losses and mass-driven sea level rise. *Geophysical Research Letters*. doi: 10.1029/2019gl082929

Loomis, B. D., Wiese, D. N., Landerer, F. W., Rachlin, K. E., & Luthcke, S. B. (2020). Replacing grace/grace-fo with satellite laser ranging: Impacts on antarctic ice sheet mass change. *Geophysical Research Letters*. doi: 10.1029/2019gl085488

Mandea, M., Narteau, C., Panet, I., & Le Mouël, J.-L. (2015). Gravimetric and magnetic anomalies produced by dissolution-crystallization at the core-mantle boundary. *Journal of Geophysical Research: Solid Earth*, *120*(9), 5983–6000. Retrieved 2022-03-11, from https://onlinelibrary.wiley.com/doi/abs/10.1002/2015JB012048 (_eprint: https://onlinelibrary.wiley.com/doi/pdf/10.1002/2015JB012048) doi: 10.1002/2015JB012048

Mandea, M., Panet, I., Lesur, V., de Viron, O., Diament, M., & Le Mouël, J.-L. (2012, November). Recent changes of the Earth's core derived from satellite observations of magnetic and gravity fields. *Proceedings of the National*

Academy of Sciences, *109*(47), 19129–19133. Retrieved 2022-03-11, from https://www.pnas.org/doi/full/10.1073/pnas.1207346109 (Publisher: Proceedings of the National Academy of Sciences) doi: 10.1073/pnas.1207346109

Marti, F., Blazquez, A., Meyssignac, B., Ablain, M., Barnoud, A., Fraudeau, R., ... Benveniste, J. (2022, January). Monitoring the ocean heat content change and the Earth energy imbalance from space altimetry and space gravimetry. *Earth System Science Data*, *14*(1), 229–249. Retrieved 2022-07-21, from https://essd.copernicus.org/articles/14/229/2022/ (Publisher: Copernicus GmbH) doi: 10.5194/essd-14-229-2022

Mayer-Gürr, T., Behzadpour, S., Ellmer, M., Klinger, B., Zehentner, N., Kvas, A., & Strasser, S. (2018). Itsg-grace2018: Monthly, daily and static gravity field solutions from grace. *null*. doi: 10.5880/icgem.2018.003

Melini, D., & Spada, G. (2019). Some remarks on Glacial Isostatic Adjustment modelling uncertainties. *Geophysical Journal International*. doi: 10.1093/gji/ggz158

Meyer, U., Lasser, M., Jaeggi, A., Dahle, C., Dahle, C., Flechtner, F., ... Bourgogne, S. (2020). International combination service for time-variable gravity fields (cost-g) monthly grace-fo series. *null*. doi: 10.5880/icgem.cost-g.002

Panet, I., Bonvalot, S., Narteau, C., Remy, D., & Lemoine, J.-M. (2018, May). Migrating pattern of deformation prior to the Tohoku-Oki earthquake revealed by GRACE data. *Nature Geoscience*, *11*(5), 367–373. Retrieved 2022-03-11, from https://www.nature.com/articles/s41561-018-0099-3 (Number: 5 Publisher: Nature Publishing Group) doi: 10.1038/s41561-018-0099-3

Peltier, W. R. (2004). Global glacial isostasy and the surface of the ice-age earth: The ice-5g (vm2) model and grace. *Annual Review of Earth and Planetary Sciences*. doi: 10.1146/annurev.earth.32.082503.144359

Peltier, W. R., Argus, D. F., & Drummond, R. (2018). Comment on "An Assessment of the ICE-6G_C (VM5a) Glacial Isostatic Adjustment Model" by Purcell et al. *Journal of Geophysical Research*. doi: 10.1002/2016jb013844

Petrov, L., & Boy, J.-P. (2004). Study of the atmospheric pressure loading signal in VLBI observations. *Journal of Geophysical Research*, *109*(B03405).

Pfeffer, J., Cazenave, A., & Barnoud, A. (2021). Analysis of the interannual variability in satellite gravity solutions: detection of climate modes in water mass displacements across continents and oceans. *Climate Dynamics*. doi: 10.1007/s00382-021-05953-z

Purcell, A., Dehecq, A., Tregoning, P., Potter, E.-K., McClusky, S. C., & Lambeck, K. (2011). Relationship between glacial isostatic adjustment and gravity perturbations observed by GRACE. *Geophysical Research Letters*, *38*(18). Retrieved 2022-03-11, from https://onlinelibrary.wiley.com/doi/abs/10.1029/2011GL048624 (_eprint: https://onlinelibrary.wiley.com/doi/pdf/10.1029/2011GL048624) doi: 10.1029/2011GL048624

Richter, H. M. P., Lück, C., Klos, A., Sideris, M. G., Rangelova, E., & Kusche, J. (2021). Reconstructing GRACE-type time-variable gravity from the Swarm satellites. *Scientific Reports*, *11*. Retrieved from https://doi.org/10.1038/s41598-020-80752-w doi: 10.1038/s41598-020-80752-w

Rodell, M., Famiglietti, J. S., Wiese, D. N., Reager, J. T., Beaudoing, H. K., Landerer, F. W., & Lo, M.-H. (2018, May). Emerging trends in global freshwater availability. *Nature*, *557*(7707), 651–659. Retrieved 2022-07-21, from https://www.nature.com/articles/s41586-018-0123-1 (Number: 7707 Publisher: Nature Publishing Group) doi: 10.1038/s41586-018-0123-1

Rodell, M., Houser, P., Jambor, U., Gottschalck, J., Mitchell, K., Meng, C.-J., ... others (2004). The global land data assimilation system. *Bulletin of the American Meteorological Society*, *85*(3), 381–394.

Rosat, S., Gillet, N., Boy, J.-P., Couhert, A., & Dumberry, M. (2021, February). Interannual variations of degree 2 from geodetic observations and surface processes. *Geophysical Journal International*, *225*(1), 200–221. Retrieved 2022-03-11, from https://doi.org/10.1093/gji/ggaa590 doi: 10.1093/gji/ggaa590

Saraswati, A. T., de Viron, O., & Mandea, M. (2022, June). *Estimation des signaux communs de la gravité spatiale et du champ magnétique liés à la variation du champ du noyau terrestre* [Poster]. Congrès national de gravimétrie spatiale du champ variable, Marseille. Retrieved 2022-07-27, from https://gravimetriefr.sciencesconf.org/browse/session?sessionid=71661

Scanlon, B. R., Zhang, Z., Save, H., Sun, A. Y., Schmied, H. M., Beek, L. P. H. v., ... Bierkens, M. F. P. (2018, February). Global models underestimate large decadal declining and rising water storage trends relative to GRACE satellite data. *Proceedings of the National Academy of Sciences*, *115*(6), E1080–E1089. Retrieved 2021-07-29, from https://www.pnas.org/content/115/6/E1080 (Publisher: National Academy of Sciences Section: PNAS Plus) doi: 10.1073/pnas.1704665115

Scanlon, B. R., Zhang, Z., Save, H., Wiese, D. N., Landerer, F. W., Long, D., ... Chen, J. (2016). Global evaluation of new grace mascon products for hydrologic applications. *Water Resources Research*, *52*(12), 9412-9429. Retrieved from https://agupubs.onlinelibrary.wiley.com/doi/abs/10.1002/2016WR019494 doi: https://doi.org/10.1002/2016WR019494

Schindelegger, M., Harker, A., Ponte, R. M., Dobslaw, H., & Salstein, D. A. (2021). Convergence of daily grace solutions and models of submonthly ocean bottom pressure variability. *Journal of Geophysical Research*. doi: 10.1029/2020jc017031

Schmeer, M., Schmidt, M., Bosch, W., & Seitz, F. (2012). Separation of mass signals within grace monthly gravity field models by means of empirical orthogonal functions. *Journal of Geodynamics*. doi: 10.1016/j.jog.2012.03.001

Schmied, H. M., Cáceres, D., Eisner, S., Flörke, M., Niemann, C., Peiris, T. A., ... Döll, P. (2020, March). *The global freshwater availability and water use model WaterGAP 2.2d* (Tech. Rep. No. EGU2020-11434). Copernicus Meetings. Retrieved 2022-07-27, from https://meetingorganizer.copernicus.org/EGU2020/EGU2020-11434.html (Conference Name: EGU2020) doi: 10.5194/egusphere-egu2020-11434

Schneider, U., Becker, A., Finger, P., Meyer-Christoffer, A., Rudolf, B., & Ziese, M. (2016). Gpcc full data reanalysis version 7.0: Monthly land-surface precipitation from rain gauges built on gts based and historic data. *null*. doi: 10.5065/d6000072

Sośnica, K., Jäggi, A., Meyer, U., Thaller, D., Beutler, G., Arnold, D., & Dach, R. (2015, October). Time variable Earth's gravity field from SLR satellites. *Journal of Geodesy*, *89*(10), 945–960. Retrieved 2021-01-25, from https://doi.org/10.1007/s00190-015-0825-1 doi: 10.1007/s00190-015-0825-1

Swenson, S., & Wahr, J. (2002). Methods for inferring regional surface-mass anomalies from gravity recovery and climate experiment (grace) measurements of time-variable gravity. *Journal of Geophysical Research*. doi: 10.1029/2001jb000576

Tapley, B. D., Bettadpur, S., Ries, J. C., Thompson, P. F., & Watkins, M. M. (2004, July). GRACE Measurements of Mass Variability in the Earth System. *Science*, *305*(5683), 503–505. Retrieved 2022-07-21, from https://www.science.org/doi/full/10.1126/science.1099192 (Publisher: American Association for the Advancement of Science) doi: 10.1126/science.1099192

Tapley, B. D., Watkins, M. M., Flechtner, F., Reigber, C., Bettadpur, S., Rodell, M., ... Velicogna, I. (2019, May). Contributions of GRACE to understanding climate change. *Nature Climate Change*, *9*(5), 358–369. Retrieved 2022-05-03, from https://www.nature.com/articles/s41558-019-0456-2 (Number: 5

Publisher: Nature Publishing Group) doi: 10.1038/s41558-019-0456-2

Velicogna, I., Mohajerani, Y., A, G., Mouginot, J., Noël, B., Sutterley, T. C., ... van Wessem, J. M. (2020). Continuity of ice sheet mass loss in greenland and antarctica from the grace and grace follow-on missions. *Geophysical Research Letters*. doi: 10.1029/2020gl087291

Wang, F., Shen, Y., Chen, Q., & Sun, Y. (2021). Reduced misclosure of global sea-level budget with updated tongji-grace2018 solution. *Scientific Reports*. doi: 10.1038/s41598-021-96880-w

Whitehouse, P. L., Bentley, M. J., Milne, G. A., King, M. A., & Thomas, I. D. (2012). A new glacial isostatic adjustment model for antarctica: calibrated and tested using observations of relative sea-level change and present-day uplift rates. *Geophysical Journal International*. doi: 10.1111/j.1365-246x.2012.05557.x

Śliwińska, J., Nastula, J., & Wińska, M. (2021). Evaluation of hydrological and cryospheric angular momentum estimates based on GRACE, GRACE-FO and SLR data for their contributions to polar motion excitation. *Earth, Planets and Space*. doi: 10.1186/s40623-021-01393-5